Design, analysis and characterization of single frequency grating-outcoupled surface emitting lasers

Taha Masood, *Member, IEEE,* Nuditha V. Amarasinghe, *Member, IEEE,* Steve Patterson, *Member, IEEE,* Scott McWilliams, *Member, IEEE,* Hanxing Shi, *Member, IEEE,* Gary A. Evans, *Fellow, IEEE,* and Jerome Butler, *Fellow, IEEE,*

***Abstract*— Design considerations for single-frequency, uncooled, 1310 nm AlGaInAs/InP grating-outcoupled surface-emitting (GSE) lasers for communications systems are presented. These GSE lasers have threshold currents of ∼20 mA at 25^{o}C, with slope efficiencies of ∼0.08 mW/mA, greater than 30 dB side-mode suppression ratios, full-width at half-maximum far-field beam divergences of 7^o x 13^o, and operate at 3.125 Gbps at temperatures up to 85^{o}C.**

***Index Terms*— Surface-emission, grating-outcouplers, distributed Bragg reflectors, semiconductor lasers.**

I. Introduction

Grating-outcoupled surface emitting (GSE) lasers have operating characteristics that include narrow beam divergence, single wavelength emission [1], high output power [2], low voltage and stable polarization. The combination of in-plane light propagation and surface normal emission make GSE lasers ideal for electronic and photonic integrated circuits [3]. Surface emission allows complete wafer level processing and testing, advantages that permitted significant reductions in cost and improved reliability for integrated circuits and short-wavelength vertical-cavity surface-emitting lasers (VCSEL) [4].

The design, fabrication and characterization of AlGaInAs/InP GSE lasers emitting at wavelengths near 1310 nm is reported. This GSE architecture is wavelength agnostic and can be applied to any existing material system used to make semiconductor lasers.

GSE lasers (Fig. 1) consist of a ridge waveguide gain section of length L_{Ridge}, distributed Bragg reflectors (DBRs) of length L_{DBR} at each end of the lasing cavity and an outcoupler of length L_{OC} placed between one of the DBR reflectors and the active ridge. The shallow DBRs provide wavelength selective feedback for single-frequency operation.

Design considerations for the GSE laser are discussed in Section II, details of the fabrication steps are in Section III and experimental results are described in Section IV.

Manuscript received June 3, 2005. This work was supported by NSF SBIR 0450560, by the Air force SBIR F29601-03-C-0026, by ATP 003613-0038-2001 and by Texas Higher Education Coordinating Board's Technology Development and Transfer Program 003613-0041-2003.

T. Masood, N. V. Amarasinghe and S. McWilliams are with Photodigm Inc..

S. Patterson is now with nLight Corporation.

H. Shi, G. A. Evans and J. Butler are with Southern Methodist University.

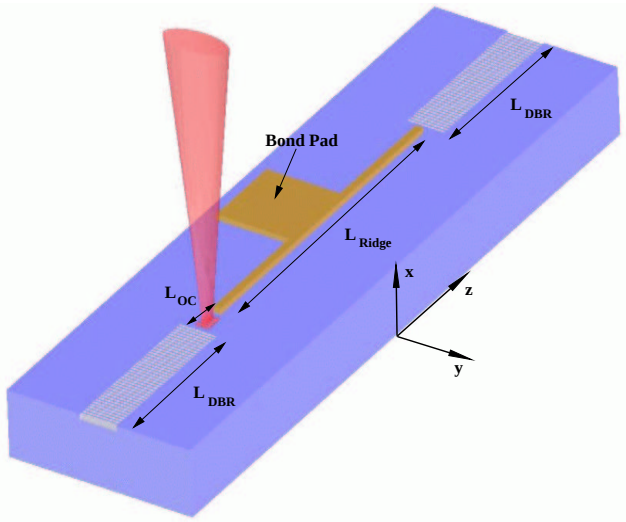

Fig. 1. The GSE semiconductor laser.

II. Design

A. Laser Structure

The modes in the GSE laser propagate along the longitudinal z direction according to $\exp\, j(\omega\, t - \beta\, z)$ where $\omega = 2\,\pi\,\nu$, ν is the photon frequency and β is the longitudinal propagation constant. The modes are analyzed using the effective index method. The optical fields are polarized along the y direction and the scalar form of the wave equation for transverse TE modes in a dielectric waveguide with l layers is

$$\frac{\partial^2 \Phi(x)}{\partial x^2} + (k_0^2 \varepsilon_i - \beta^2)\Phi(x) = 0, i = 1, 2, ...l \qquad (1)$$

where Φ is the electric field, k_0 is the free-space wavenumber and ε_i is the dielectric constant of the ith dielectric layer..

The quantum well confinement factor Γ_w is the fraction of the modal power contained in each quantum well (QW) and is defined as

$$\Gamma_w = \frac{\int_{\mathrm{QW}} \Phi^2(x) dx}{\int \Phi^2(x) dx} \qquad (2)$$

The fabricated 1310 nm GSE lasers used the basic high speed, uncooled structure [5], [6] shown in Table I. Edge-emitting lasers using this structure have a minimum threshold current for a cavity length of ∼400 μm at 85^o C [6].

The epitaxial structure is composed of five quantum wells, four barriers, two graded-index (GRIN) layers, two seperate confinement heterostructure (SCH) layers, two transition

TABLE I
LASER COMPOSITION AND THICKNESS FOR 1310-NM LASER STRUCTURE

Layer	Composition		Thickness (μm)
n-substrate	InP		0.5
n-transition GRIN	$Al_{0.41}Ga_{0.067}In_{0.52}As$–$Al_{0.48}In_{0.52}As$		0.01
n-SCH	$Al_{0.48}In_{0.52}As$	t_{SCH}	0.011
n-GRIN	$Al_{0.48}In_{0.52}As$–$Al_{0.26}Ga_{0.22}In_{0.52}As$	t_{GRIN}	0.15
5x QW	$Al_{0.16}Ga_{0.12}In_{0.71}As$		0.005
4x barrier	$Al_{0.26}Ga_{0.22}In_{0.52}As$		0.01
p-GRIN	$Al_{0.26}Ga_{0.22}In_{0.52}As$–$Al_{0.48}In_{0.52}As$	t_{GRIN}	0.15
p-SCH	$Al_{0.48}In_{0.52}As$	t_{SCH}	0.011
p-transition GRIN	$Al_{0.48}In_{0.52}As$–$Al_{0.41}Ga_{0.067}In_{0.52}As$		0.01
p-spacer (grating)	InP	t_{spacer}	0.12
etch stop	InGaAsP		0.01
p-clad	InP	t_{clad}	1.3
p-cap	InGaAs	t_{cap}	0.19

GRIN layers, one p-spacer layer, an etch stop layer, cladding layer and an InGaAs cap layer. The index profile and field distribution for the epitaxial structure shown in Table I are plotted in Fig. 2. The layer thicknesses for the SCH and GRIN layers (Table I) were determined using WAVEGUIDE [7] to simultaneously maximize the quantum well confinement factor (Fig. 3) and the grating layer confinement factor (Fig. 4) as a function of the thicknesses of the GRIN and SCH layers.

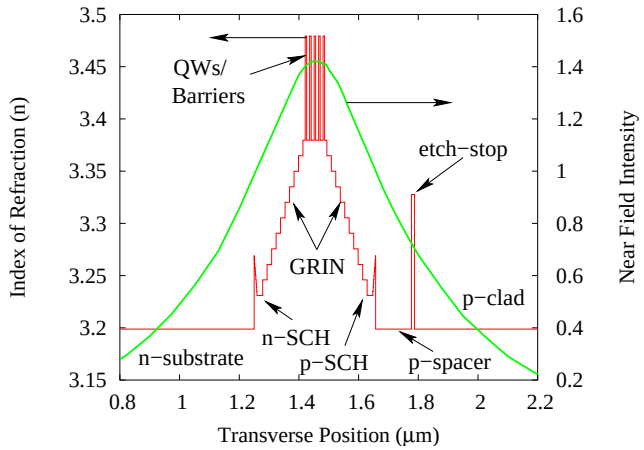

Fig. 2. Transverse index of refraction and near-field intensity profile of the epitaxial structure.

Figure 5 shows the modal losses due only to the highly doped (1x10^{19} Zn atoms/cm^3) p-cap layer and the p-cap metalization (TiPtAu) as a function of p-clad thickness. A p-clad layer thickness of 1300 nm was chosen to provide acceptable losses. The lateral index step for a ridge waveguide (Fig. 6) as a function of p-spacer thickness is shown in Fig. 7. The desired lateral index step Δn of ∼0.015 [6] is determined by the position of the InGaAsP etch stop layer.

The calculated transverse modes in the ridge, transition and grating regions of the epitaxial structure as the wave propagates from the ridge to the grating region are shown in Fig. 8. An intensity overlap [4] approaching 100% between

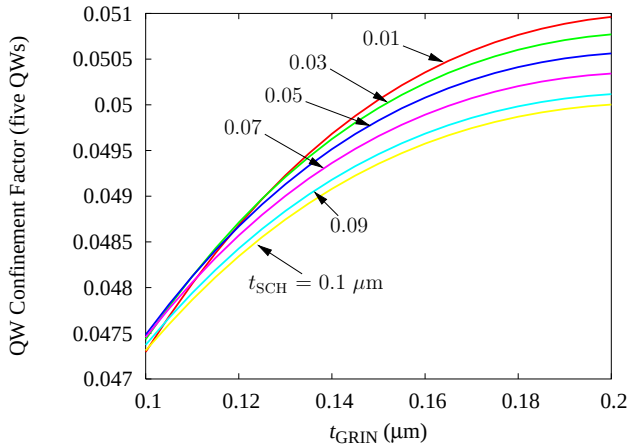

Fig. 3. Quantum well confinement (five QWs) vs. GRIN layer thickness for multiple SCH layer thicknesses. Both n and p side layers are varied simultaneously.

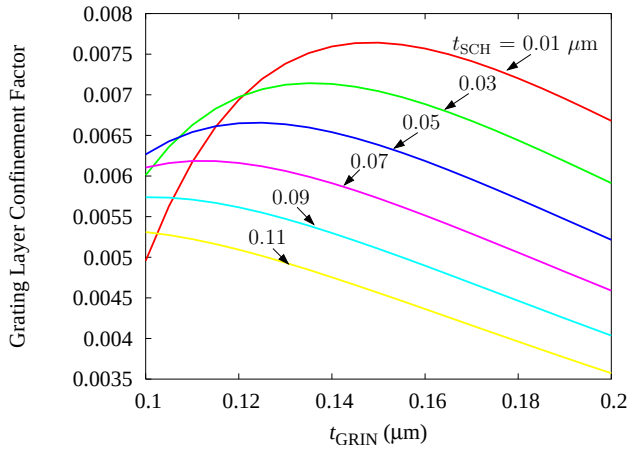

Fig. 4. Grating layer confinement factor vs. GRIN layer thickness for multiple SCH layer thicknesses. Both n and p side layers are varied simultaneously.

the modes in the three regions is desired for low threshold, high efficiency devices. For lateral mode control, a lateral index of ∼0.01 to 0.015 is required to offset the gain-induced index depression [8] for long-wavelength lasers, which results in lower (∼80 to 90%) intensity overlaps between the ridge and grating regions. A solution to this problem is the use of separate etch stops to locate the gratings and the bottom of the channels on either side of the ridges.

Table II shows the modal intensity overlaps between the ridge and the channel region and the ridge and grating region for different p-spacer (grating) layer thicknesses and the resulting lateral index step.

B. DBR Design

Rectangular gratings with ∼50% duty cycle are etched into the InGaAsP etch-stop and InP p-spacer layers (Fig. 8) with a period of Λ and depth of h.

The reflectivity of the first-order DBR gratings are calculated using the coupled mode theory [9] [10]. The coupling coefficient κ is given by

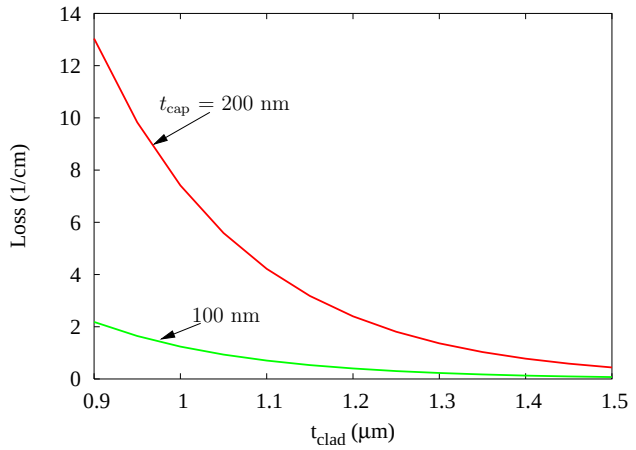

Fig. 5. Modal loss (1/cm) vs. p-clad thickness. Only the losses due to cap layer doping and metal losses are included.

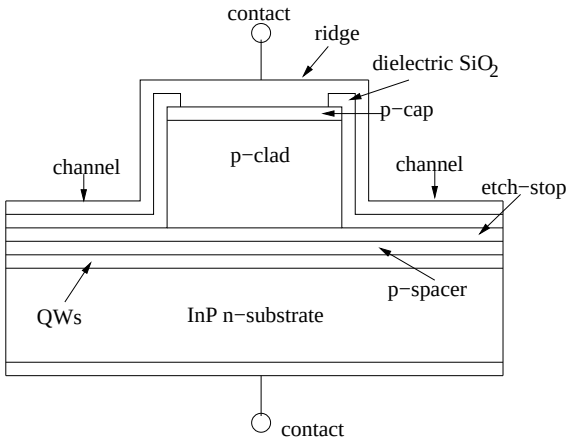

Fig. 6. Cross section of the ridge.

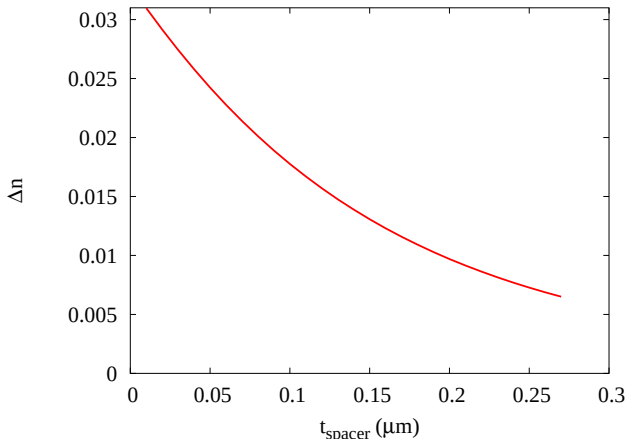

Fig. 7. The lateral index step as a function of p-spacer thickness.

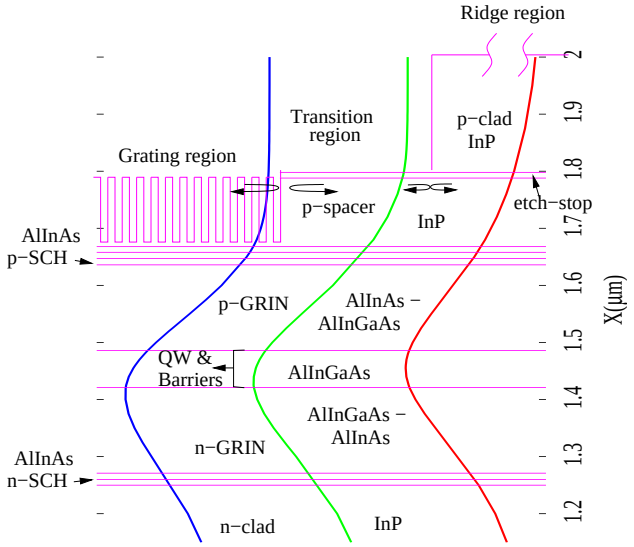

Fig. 8. Calculated transverse mode intensity in the ridge, transition and grating regions of the epitaxial structure.

$$\kappa = \frac{k_0^2}{2\beta}\int_{corrugation} \triangle[n^2(x,z)]\Phi^2(x)dx \tag{3}$$

where Φ is the normalized y-component of the E-field satisfying

$$1 = \int_{-\infty}^{\infty} \Phi^2(x)dx \tag{4}$$

$\triangle[n^2(x,z)]$ is the perturbation in the refractive index ($n^2(x,z)$ is the refractive index in the grating layer). For a grating section of length L_{DBR}, the reflection and transmission coefficients r and t are given by [11]

$$r = \frac{-\kappa^* \sinh SL_{\mathrm{DBR}}}{\triangle\beta \sinh SL_{\mathrm{DBR}} + iS\cosh SL_{\mathrm{DBR}}} \tag{5}$$

$$t = \frac{iS}{\triangle\beta \sinh SL_{\mathrm{DBR}} + iS\cosh SL_{\mathrm{DBR}}} \tag{6}$$

where $S = \sqrt{|\kappa|^2 - (\triangle\beta)^2}$, $\triangle\beta = \beta - \frac{\pi}{\Lambda}$ is the detuning parameter.

Reflectivities for 62, 100 and 200 μm long rectangular and triangular DBR gratings with a depth of 0.13 μm are plotted as a function of the detuning parameter in Figs. 9 and 10. The reflectivities of a sinusoidal grating fall between these extremes. These plots show that 100 μm long DBR gratings have a peak reflectivity of greater than 90%, ignoring scattering loss due to grating sidewall roughness and coupling loss between the DBR and the ridge.

TABLE II

TRANSVERSE MODE INTENSITY OVERLAP INTEGRALS BETWEEN RIDGE AND THE CHANNEL REGION AND THE RIDGE AND GRATING REGION.

p-spacer thickness (μm)	**Intensity Overlap (ridge/channel)**	**Intensity Overlap (ridge/grating)**	**Lateral Index Step**
0.05	0.85	0.81	0.024
0.1	0.89	0.82	0.018
0.15	0.92	0.83	0.013

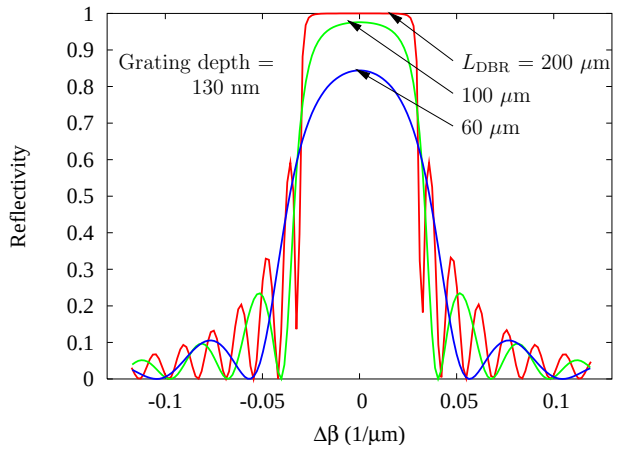

Fig. 9. DBR reflectivity vs. detuning parameter for 62, 100, and 200 μm long DBR section with rectangular grating teeth profile.

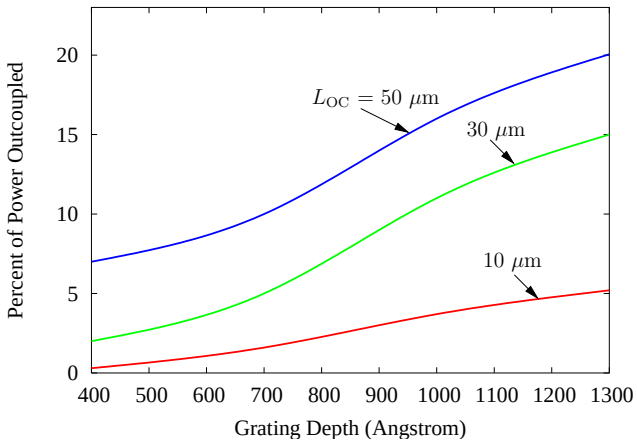

Fig. 11. Percent of power outcoupled vs. grating depth for 10, 30 and 50 μm long outcouplers.

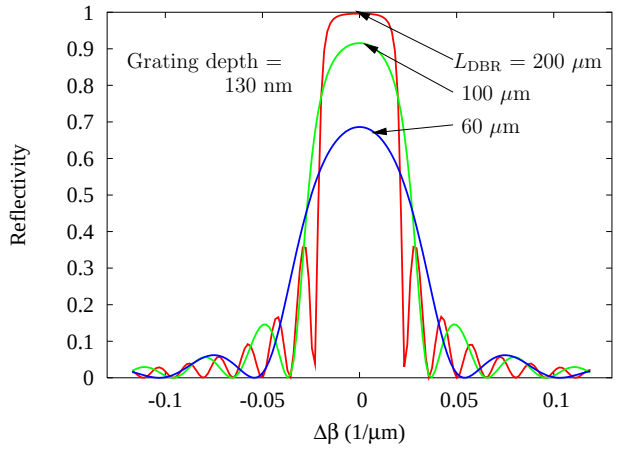

Fig. 10. DBR reflectivity vs. detuning parameter for 62, 100, and 200 μm long DBR section with triangular grating teeth profile.

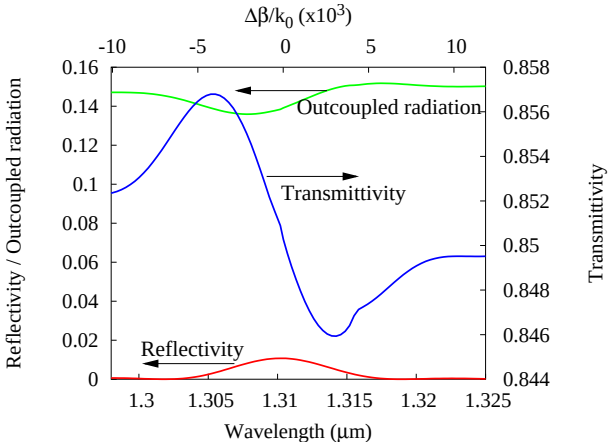

Fig. 12. Power outcoupled, radiated, transmitted vs. wavelength for a 30 μm long outcoupler. The Bragg (resonance) wavelength is 1.31 μm.

C. Outcoupler Design

The outcoupler grating was analyzed using a Floquet-Bloch approach [2] [12] [13] [14] to determine the reflected, transmitted and outcoupled power for a finite length grating. The grating outcoupler corresponds to the layers shown in Fig. 8 with the corresponding layer compositions and thicknesses given in Table I.

Figure 11 shows the percent of incident power that is radiated (up and down) on-resonance as a function of grating depth for 10, 30 and 50 μm long outcouplers. For a second order grating depth of 1300 Angstrom, the on-resonance outcoupled power is 5, 15, and 20% for a 10, 30 and 50 μm long outcoupler respectively.

The reflectivity of the second order grating peaks on-resonance (Fig. 12). Figure 13 shows that on-resonance the reflectivity per pass from a 50 μm long and 1300 Angstrom deep second-order grating outcoupler is about 2%.

The reflectivity from the second-order grating can be minimized by detuning the second order grating period from the DBR selected wavelength. Figure 12 shows that the second order grating outcoupler of length 30 μm is not reflective if the grating period of the second order grating outcoupler is detuned by $\geq \pm 20$ Angstrom (or 6 nm in wavelength). The same plot also shows a dip in the outcoupled power close to the Bragg wavelength.

So far, the outcoupler radiation has been considered only for a Bloch wave propagating in one direction. In these GSE lasers, the outcoupler is inside the laser cavity, colocated with a standing wave set up by the counter propagating Bloch waves.

The alignment of the outcoupler grating teeth with respect to the standing wave affects the fraction of light outcoupled. Figure 14 [15] shows two cases corresponding to when the grating teeth are in-phase (symmetric mode) or out-of-phase (antisymmetric mode) with respect to the standing wave. On-resonance the symmetric mode radiates maximum power while the antisymmetric mode radiates no power. The outcoupler radiates a varying fraction of the maximum power for phase (φ) values that lie between the symmetric (0^o) and antisymmetric phase (180^o).

Due to changes of the effective index with drive current and temperature, the phase of the standing wave with respect to the outcoupler grating may change. This may result in kinks

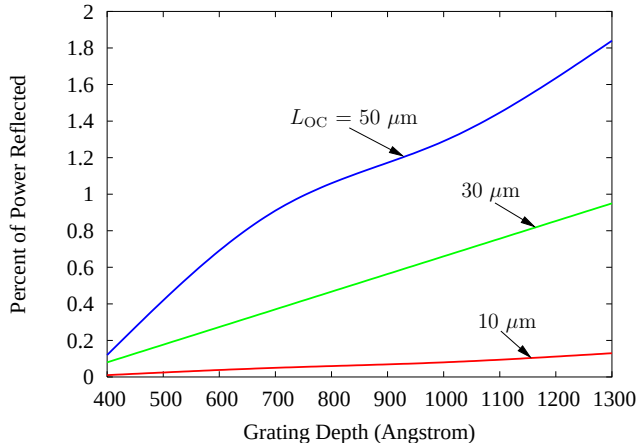

Fig. 13. Percent of power reflected vs. grating depth for 10, 30, 50 μm long outcouplers.

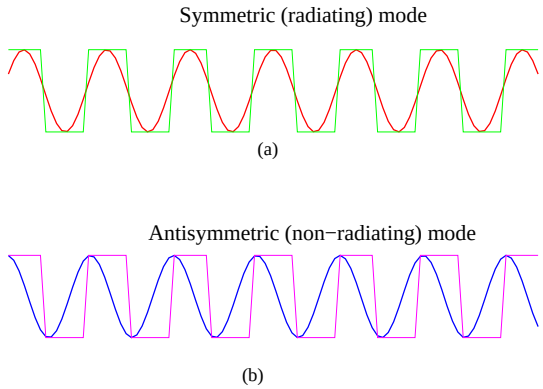

Fig. 14. On resonance waveguide field for the (a) symmetric and (b) antisymmetric infinite standing wave solutions along the longitudinal coordinate. The symmetric mode is radiating while the antisymmetric mode is nonradiating for the on-Bragg condition [15].

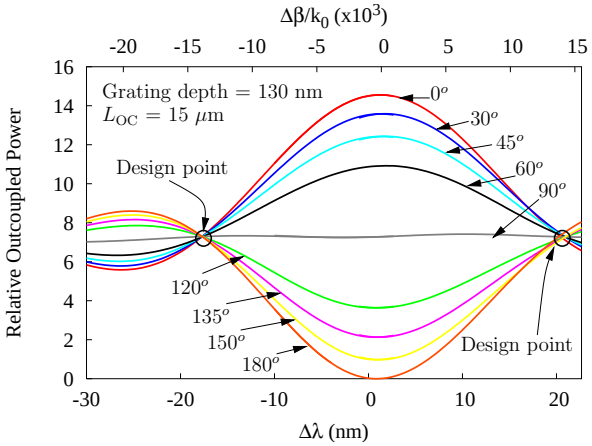

Fig. 15. Relative outcoupled power vs. detuning from the Bragg wavelength and relative phase between counter propagating waves for a 15 μm long outcoupler.

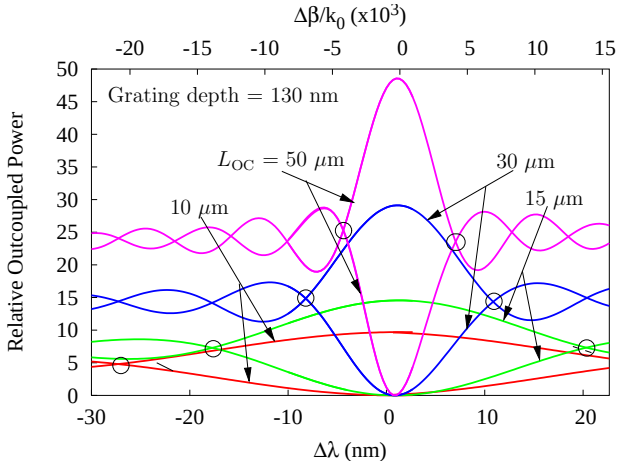

Fig. 16. Relative outcoupled power of symmetric and antisymmetric mode vs. detuning from the Bragg wavelength for a 10, 15, 30, and 50 μm long outcoupler.

in the LI curve [16] [17] if the grating is on resonance. These kinks may be avoided by detuning the outcoupler from the resonance condition.

Figure 15 calculates the relative outcoupled power from a 15 μm long GSE outcoupler as a function of detuning ($\Delta\lambda$) from the Bragg resonance as the input phase at one end of the grating is varied, assuming that the field amplitudes are equal at both inputs to the grating. This plot, calculated using Floquet Bloch theory [2] [12] [13] [14], indicates that if the outcoupler is detuned $\sim \pm 18$ nm, the outcoupled intensity is insensitive to phase variations.

Figure 16 shows the relative outcoupled power of symmetric and antisymmetric mode as a function of the detuning ($\Delta\lambda$) from the Bragg wavelength for 10, 15, 30, and 50 μm long outcouplers. This plot shows that the detuning points at which the outcoupled power becomes insensitive to the phase differences move closer to the exact Bragg condition as the outcoupler length increases.

If the input amplitudes of the optical fields at each end of the grating are not equal, less power is outcoupled if both input waves are in phase, and a non-zero amount of power is outcoupled if both waves are π out of phase. Figure 17 shows in-phase and out-of-phase outcoupling for amplitude-balanced inputs and for amplitude inputs that differ by a factor of two.

Figure 18 shows the near-field intensity of the outcoupler for different relative phases between the counter propagating beams exciting the outcoupler, when the outcoupler is on resonance. The light outcoupled monotonically decreases as the standing wave moves from in-phase to out-of-phase with respect to the outcoupler grating teeth.

Figure 19 shows the corresponding far-field intensity patterns for the phase difference values shown in Fig. 18. The far-field profiles stay single-lobed for almost all phase difference values except when the phase is 180^o, in which case the far-field becomes dual-lobed. When the phase difference is close to 180^o, the power outcoupled is essentially zero.

The power outcoupled is insensitive to phase difference variations when the emission wavelength is detuned from the outcoupler resonance by $\sim \pm 18$ nm (Fig. 15). However, the near-field intensity patterns change significantly with phase difference changes, from having most of the intensity at the

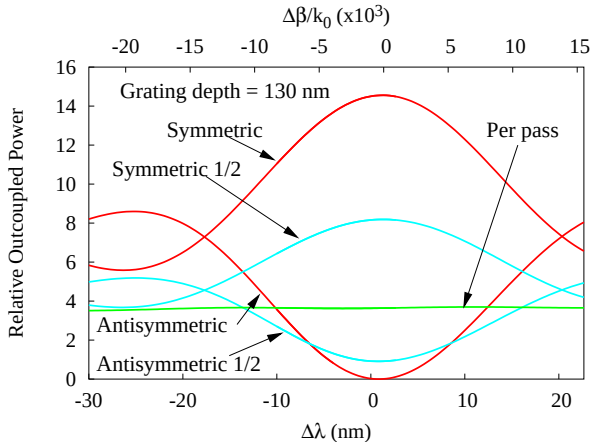

Fig. 17. Relative outcoupled power of symmetric and antisymmetric mode vs. detuning from the Bragg wavelength for optical waves input amplitudes that are either equal or differ by a factor of 2. The relative outcoupled power for wave propagating only in one direction (per pass) is also shown as reference. The outcoupler is 15 μm long.

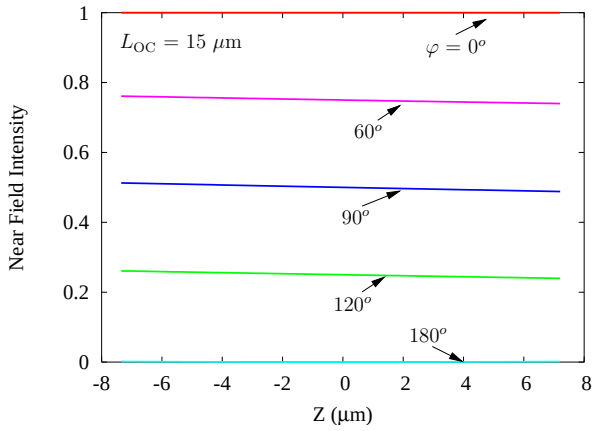

Fig. 18. On-Bragg near-field profiles for various relative phases of the counter propagating waves exciting the outcoupler.

center, to having a null in the center with most of the intensity at both ends of the outcoupler as shown in (Fig. 20). The far-field profiles may have one or two lobes, depending on the phase (Fig. 21).

The outcoupler radiates power into the air as well as the substrate. Although not incorporated in the present devices, a reflector located above [4] or below the waveguide can redirect most of the radiated power in one direction, thus increasing the outcoupled power [2].

The theoretical results of this section show that operating on-resonance provides stable near- and far-fields with respect to phase changes. However, the fraction of light outcoupled from an on-resonance grating is sensitive to phase changes and can result in kinks in the light-current curves. The sensitivity of the light-current curve to phase changes can be exploited by integrating a phase shifter section to the device to act as a modulator while maintaining the current to the gain region at a constant value.

Detuning the outcoupling grating (Figs. 15 and 16) is an approach to light-current curves that are insensitive to phase

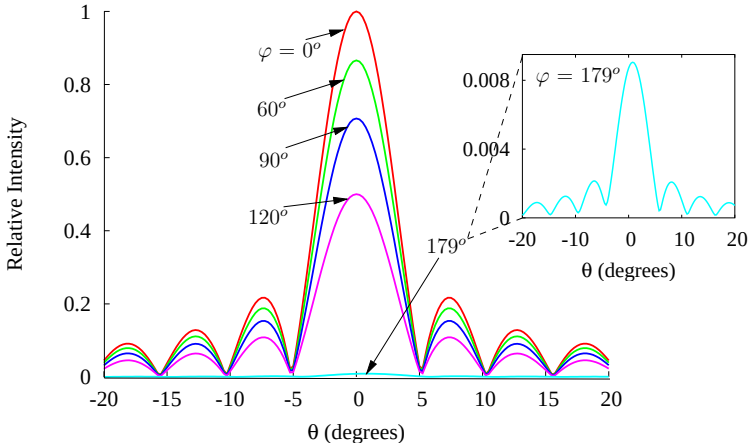

Fig. 19. On-Bragg far-field profiles for various relative phases of the counter propagating waves exciting the outcoupler.

changes. The drawback with this approach is that the near-field intensity distribution across the grating shifts with phase. As a result, when the GSE laser is coupled into a fiber, kinks in the power coupled into a fiber may occur, especially with single-mode fiber.

III. Fabrication

The ridge-guide, DBR and the outcoupler regions are defined by etching away the p-cap and p-clad layers down to the etch stop layer in the present device (Fig. 22). A holographic lithography process defines a photoresist grating pattern with a 0.2074-μm period in the DBR regions and a 0.42-μm period in the outcoupler region. Reactive ion etching is used to transfer the photoresist grating into the underlying semiconductor. The resulting gratings have a depth of $\sim$130 nm for both the first and second-order gratings. After etching the DBR gratings a shallow (0.05 μm) ridge is etched in the DBR regions for lateral mode control and the device is passivated by 200 nm of silicon oxide.

IV. Experimental Results

GSE lasers were probe-tested under continuous-wave operation at the wafer level and then mounted on TO-46 or TO-56 headers. The light-current-voltage (LI-V) characteristics into a broad-area detector (Fig. 23) show linear L-I curves over the temperature range of 25 to 85^{o}C for a GSE laser with an outcoupler grating period that is detuned by +18 nm. The "snap-on" behavior near threshold of the L-I curve at 85^{o}C is due to saturable absorption in the DBR and outcoupler regions and can be eliminated by increasing the bandgap in the passive DBR regions by quantum well intermixing [18]. The reflectivities of the DBRs are $\sim$45% and were determined by comparison with the thresholds of Fabry-Perot ridge-waveguide lasers made from the same wafer with identical gain section dimensions. Reducing radiation losses by increasing the overlap of the fields between the end of the ridges and the DBR passive regions by increasing the thickness of p-spacer layer (Table II) is expected to increase the DBR reflectivity to more than 80%. Increases in the DBR

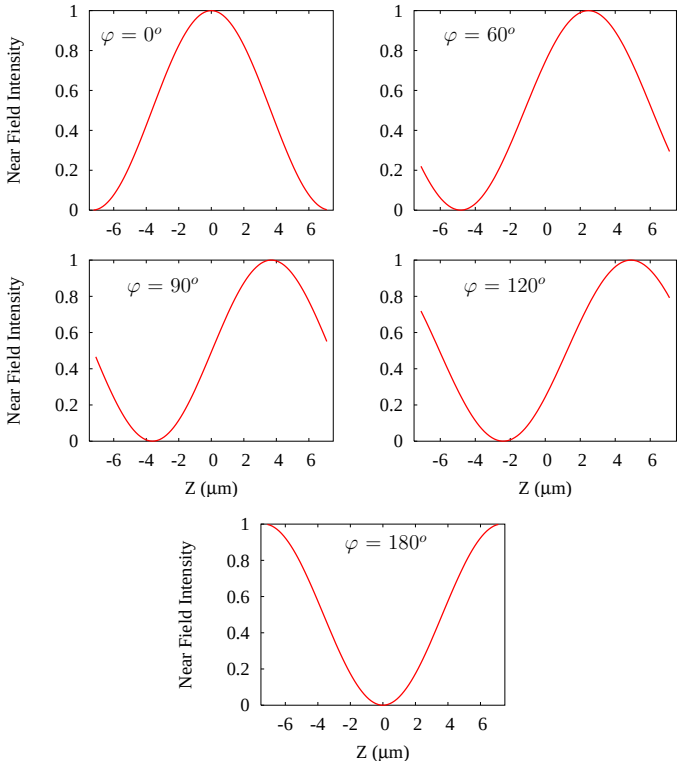

Fig. 20. Simulated near-field profiles for 18 nm detuned and 15 μm long outcoupler for various relative phases of the counter propagating waves exciting the outcoupler.

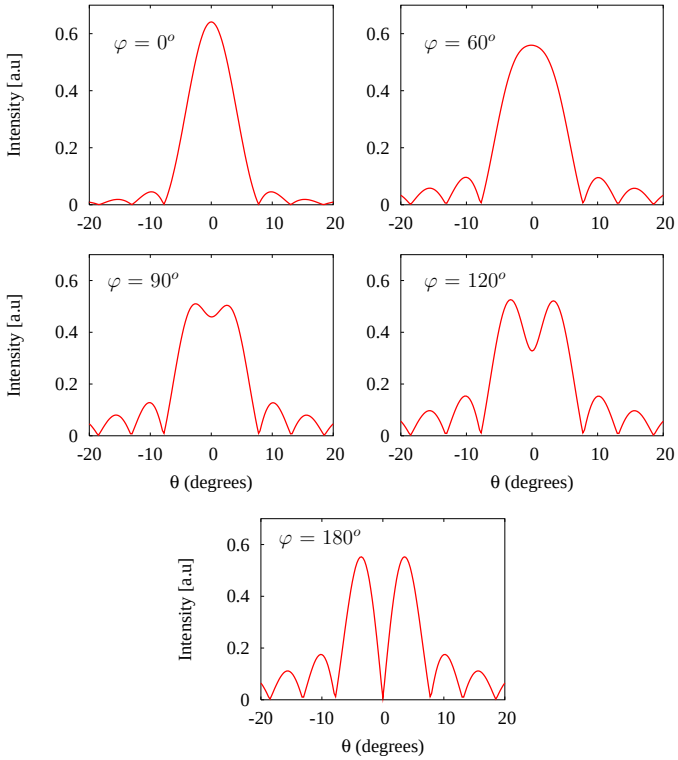

Fig. 21. Simulated far-field profiles for 18 nm detuned and 15 μm long outcoupler for different relative phases of the counter propagating waves exciting the outcoupler.

reflectivities and the addition of a reflector over the grating will reduce the thresholds to below 10 mA and increase the slope of the L-I curves to ∼0.2 to 0.3 mW/mA.

Side-mode suppression ratios (SMSR) and wavelength shifts as a function of current at different temperatures are shown in Figs. 24 and 25 respectively. The near- and single-lobe far-field of an 18 nm detuned 15 μm long outcoupler are shown in Fig. 26. GSE lasers with detuned outcouplers operating at different temperatures and currents may exhibit different near- and far-field profiles. The full-width at half maximum (FWHM) far-field beam divergence is 7^o x 13^o for a 15 μm long outcoupler.

L-I curves from mounted lasers butt-coupled (no lenses) to multi-mode or single-mode fiber are shown in Fig. 27 and show ∼85% coupling to multi-mode fiber and ∼40% coupling to single-mode fiber.

Figure 28 shows an 3.125 Gb/s eye diagram for a DC coupled GSE laser biased at 30 mA driven by a NRZ $2^{23}-1$ back-to-back pseudorandom signal with a modulation depth of 50 mA. The measured rise time was 71 ps and the fall time was 138 ps.

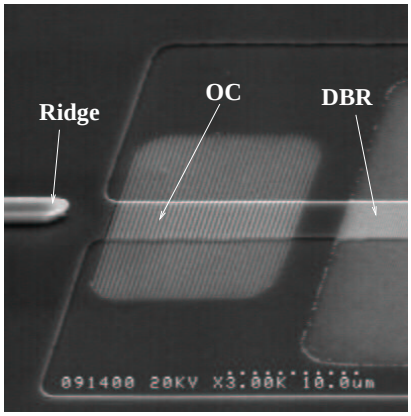

Fig. 22. Ridge, second-order outcoupler, and first-order DBR gratings. The ridges in the outcoupler and DBR sections are also etched for lateral mode confinement.

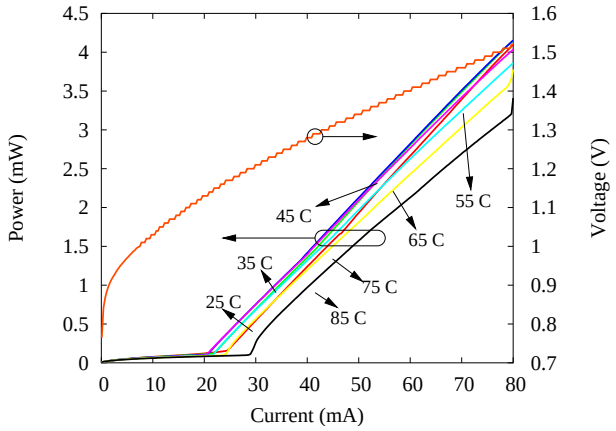

Fig. 23. High temperature LIV characteristics of a GSE laser with 400 μm long ridge, 200 μm long DBRs, and 15 μm long and 18 nm detuned outcoupler.

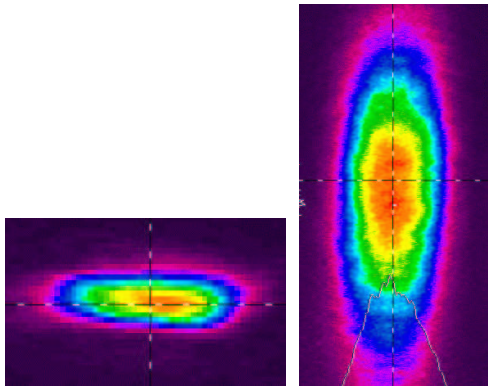

Fig. 26. Near-field (a) and Far-field (b) of 15 μm long outcoupler operating on symmetric mode. The FWHP beam divergence is 7^o x 13^o.

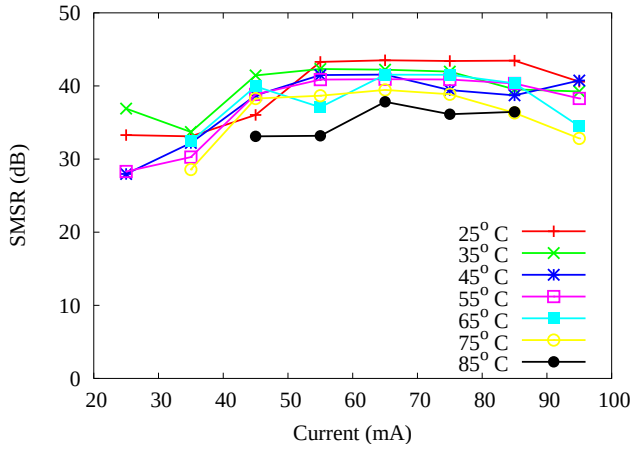

Fig. 24. Measured SMSR vs. current and temperature.

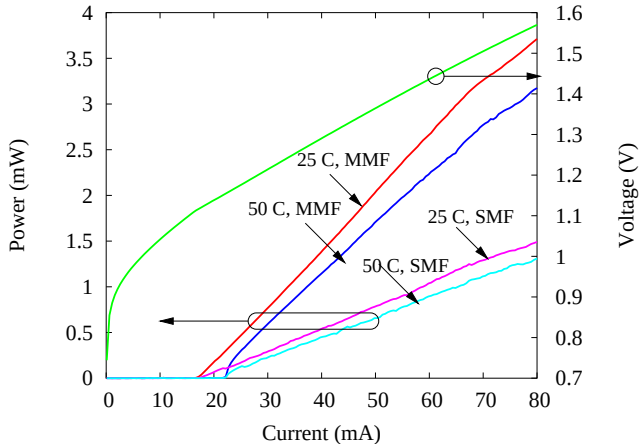

Fig. 27. LIV (CW) characteristics of GSE laser butt-coupled to single-mode and multi-mode fiber at 25^oC and 50^oC.

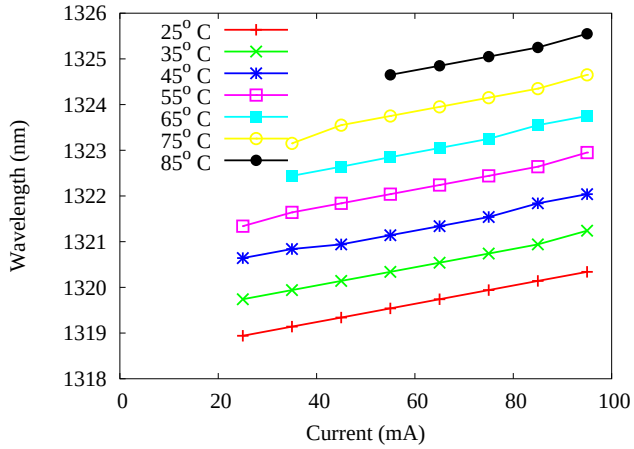

Fig. 25. Measured wavelength vs. current and temperature.

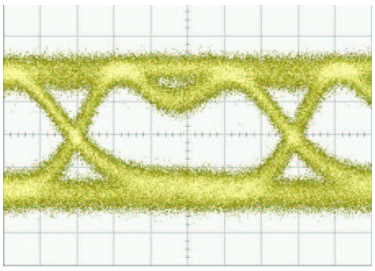

Fig. 28. Open eye diagram at 3.125Gb/s modulation rate for a GSE laser with a 15 μm long outcoupler. $I_{\rm bias}$ = 30 mA and $I_{\rm mod}$ = 50 mA. The rise time = 71 ps and fall time = 138 ps. The GSE laser is driven by a pseudorandom NRZ $2^{23}-1$ back-to-back signal.

V. Conclusion

Design considerations and experimental results for prototype single-frequency GSE datacom lasers consisting of wavelength selective first-order DBR feedback gratings and second-order outcoupler gratings were presented. Operation of the outcoupler on-resonance results in a stable, single-lobed output beam. However, the fraction of the outcoupled power varies with changes in the relative phase of the waves exciting the outcoupler. The phase sensitivity of the outcoupled power can be eliminated by appropriate detuning of the outcoupler grating period with respect to the DBR grating period, but with an associated penalty of shift in the near-field intensity distribution with relative phase shifts of the two waves exciting the outcoupler. Since such near-field distribution shifts can effect the coupling efficiency into single mode fiber, an outcoupling grating that simultaneously has a stable near-field and outcouples a fixed fraction of the optical power in the presence of phase shifts is desired. An alternative approach is to use a GSE laser with an on-resonance outcoupler and an internal phase shifter to provide a modulated output.

Prototype GSE lasers with detuned outcouplers operate at 85^{o}C and demonstrate slope efficiencies exceeding 0.08 mW/mA, threshold currents in the 20 to 25 mA range, greater than 30-dB side mode suppression ratios and have an open eye pattern for a NRZ signal at 3.125 Gb/s. The far-field beam divergence measured at FWHM is 7^o x 13^o for a 15 μm long outcoupler. Improvements in the DBR reflectivity (from $\sim$45% to $>$ 80%) along with quantum well intermixing of the passive DBR and outcoupler regions are expected to significantly improve the performance of these devices.

Acknowledgment

The authors would like to thank N. Bhandarkar, J. Castillega, C. Xiang, D. Perry, D. Roh, N.Clay and J. Kirk for their support.

References

[1] T. Masood, S. Patterson, N. V. Amarasinghe, S. McWilliams, D. Phan, D. Lee, Z. A. Hilali, X. Zhang, and G. A. Evans, "Single frequency 1310-nm algainas-inp grating-outcoupled surface-emitting lasers," *IEEE Photon. Technol. Lett.*, vol. 28, pp. 732–734, 2004.

[2] G. A. Evans, D. P. Bour, N. W. Carlson, R. Amantea, J. M. Hammer, H. Lee, M. Lurie, R. C. Lai, P. F. Pelka, R. E. Farkas, J. B. Kirk, S. K. Liew, W. F. Riechert, C. A. Wang, H. K. Choi, J. N. Walpole, J. K. Butler, W. F. Ferguson, R. K. DeFreez, and M. Felisky, "Characteristics of coherent two-dimensional grating surface emitting diode laser arrays during cw operation," *IEEE J. Quantum Electron.*, vol. 27, pp. 1594–1605, 1991.

[3] N. Eriksson, M. Hagberg, and A. Larsson, "Highly efficient grating-coupled surface-emitters with single outcoupling elements," *IEEE Photon. Technol. Lett.*, vol. 7, pp. 1394–1396, 1995.

[4] G. A. Evans and J. M. Hammer, *Surface emitting semiconductor lasers and arrays*. San Diego, C.A.: Academic Press, Inc., 1993.

[5] C. E. Zah, R. Bhat, B. N. Pathak, F. Favire, W. Lin, M. C. Wang, C. Andreadakis, D. M. Hwang, M. A. Koza, T. P. Lee, Z. Wang, D. Darby, D. Flanders, and J. J. Hsieh, "High-performance uncooled 1.3-μm AlGaInAs/InP strained-layer quantum-well lasers for subscriber loop applications," *IEEE J. Quantum Electron.*, vol. 30, pp. 511–521, 1994.

[6] S. R. Selmic, T. M. Chou, J. P. Sih, J. B. Kirk, A. Mantie, J. K. Butler, D. Bour, and G. A. Evans, "Design and characterization of 1.3-μm AlGaInAs-InP multiple quantum well lasers," *IEEE J. Selected Topics in Quantum Electron.*, vol. 5, pp. 340–349, 2001.

[7] R. Smith and G. Mitchell, *Calculation of complex propagation modes in arbitrary, plane-layered, complex dielectric structures*. Seattle, WA, EE Techical Rep.206: Univ. Washington, 1977.

[8] J. Manning, R. Olshansky, and C. B. Su, "The carrier-induced index change in AlGaAs and 1.3 μm InGaAsP diode lasers," *IEEE J. Quantum Electron.*, vol. 19, pp. 1525–1530, 1983.

[9] A. Yariv, "Coupled-mode theory for guided-wave optics," *IEEE J. Quantum Electron.*, vol. 9, pp. 919–933, 1973.

[10] W. Streifer, D. Scifres, and R. Burnham, "Coupling coefficients for distributed feedback single- and double-heterostructure diode lasers," *IEEE J. Quantum Electron.*, vol. 11, pp. 867–873, 1975.

[11] S. L. Chuang, *Physics of Optoelectronic Devices*. Wiley Series in Pure and Applied Optics, 1995.

[12] J. Tausch and J. Butler, "Efficient analysis of periodic dielectric waveguides using Dirichlet-to-Neumann maps," *J. Opt. Soc. Am.*, vol. 19, pp. 1120–1128, 2002.

[13] G. Hadjicostas, J. K. Butler, G. A. Evans, N. W. Carlson, and R. Amantea, "A numerical investigation of wave interactions in dielectric waveguides with periodic surface corrugations," *IEEE J. Quantum Electron.*, vol. 26, pp. 893–902, 1990.

[14] J. K. Butler, W. F. Ferguson, G. A. Evans, P. J. Stabile, and A. Rosen, "A boundary element technique applied to the analysis of waveguides with periodic surface corrugations," *IEEE J. Quantum Electron.*, vol. 28, pp. 1701–1709, 1992.

[15] R. J. Noll and S. H. Macomber, "Analysis of grating surface emitting lasers," *IEEE J. Quantum Electron.*, vol. 26, pp. 456–466, 1990.

[16] S. Bonnefont, B. Dagens, P. Arguel, H. Martinot, and F. Lozes-Dupuy, "Analysis of the sensitivity of grating-coupled surface-emitting lasers to geometrical parameter variations," *IEEE J. Quantum Electron.*, vol. 32, pp. 1469–1477, 1996.

[17] J. S. Major and D. F. Welch, "Singlemode InGaAs/GaAs distributed Bragg reflector laser diodes operating at 1083 nm," *Electron. Lett.*, vol. 29, pp. 2121–2122, 1993.

[18] B. C. Qiu, X. F. Liu, M. L. Ke, H. K. Lee, A. C. Bryce, J. S. Aitchison, J. H. Marsh, and C. B. Button, "Monolithic fabrication of 2 x 2 crosspoint switches in InGaAs-InAlGaAs multiple quantum wells using quantum-well intermixing," *IEEE Photon. Technol. Lett.*, vol. 13, pp. 1292–1294, 2001.

PLACE PHOTO HERE

Taha Masood Taha Masood has an M.S. in Electrical Engineering, Southern Methodist University, 2000 and is a PhD candidate in Electrical Engineering. Taha Masood is the Director of Engineering and Strategic Business Development at Photodigm Inc. After getting his B.S. in Electrical Engineering and B.A. in Applied Mathematics from University of Buffalo in 1990, he worked as a Project Leader and Senior Engineer at Xerox, New York during 1991-1995 and as a Project Leader and Electrical Design Engineer at Texas Instruments, Dallas during 1996-2000.

PLACE PHOTO HERE

Nuditha Vibhavie Amarasinghe Dr. Nuditha Vibhavie Amarasinghe received a B.S. degree in Physics with honors from University of Colombo, Sri Lanka in 1993 and served in the academic staff in the Department of Physics at the same university from 1993 to 1996. He received a M.S. degree in Physics from Wichita State University, Wichita, KS in 1998 and Ph.D in Electrical Engineering from Southern Methodist University, Dallas, TX in 2001. He has authored or co-authored nine journal publications, seven conference proceedings, a book chapter, and three patents. Dr. Amarasinghe is principal engineer at Photodigm Inc..

PLACE PHOTO HERE

Steve Patterson Steve Patterson was born in Philadelphia, Pa. After nine years service as a U.S. Army Ranger, he received the S.M. degree in 1995 and the Ph.D. degree in 2000, both in electrical engineering, from the Massachusetts Institute of Technology, Cambridge, MA. He worked as an R&D engineer at Agilent Technologies, San Jose, Ca. from 2000 to 2001. At Agilent, he worked on 2.5 Gbps, 1X12 arrays of vertical cavity surface emitting lasers. At Photodigm, he served as Vice President, Engineering and Principal Engineer, leading the research, development and manufacturing efforts for the first grating-coupled surface emitting lasers designed for use in data and telecom applications. Dr. Patterson left for nLight Photonics, Vancouver, WA., in 2004 where he serves as Principal Scientist, researching all aspects of high-power lasers.

PLACE PHOTO HERE

Scott McWilliams Scott McWilliams received the M.S degree in Electronic Materials and Devices from San Jose State University, San Jose, Ca, 1996. He focused on epitaxial diamond growth and device fabrication, radiation tolerant electronic devices, and laser diode heat-sinks at Crystallume Corporation, Menlo Park, Ca (1990-1994). In 1994, Scott joined Lam Research as a Senior Process Engineer where he developed high density plasma dry etch processes for high volume silicon manufacturing for 4 years. In 2000, Scott joined nLight Photonics, Vancouver, WA as a Member of the Technical Staff to help build the laser manufacturing facility from the ground up and develop high power laser diode arrays. Currently Scott is serving as the Director of Operations at Photodigm Corporation where he is responsible for manufacturing laser diodes.

PLACE PHOTO HERE

Hanxing Shi Hanxing Shi was born in Inner Mongolia, China. She received the B.S. degree in physics from Beijing Normal University, Beijing, China in 1994 and the Ph.D degree in electrical engineering from Beijing University of Posts and Telecommunications, Beijing, China in 1999. From 1999 to 2001, she worked as an assistant research engineer at the Optical Technology Center in the University of California, Santa Barbara, California, where her fields of interest were optical properties of III-V semiconductor lasers. In 2002, as a technical staff of optics in Yotta Networks, Inc., Dallas, Texas, she primarily worked on developing a multi-terabit telecommunication metro crossconnect subsystem with a photonics based switch fabric. Since 2003, she is a postdoctoral research fellow in the Department of Electrical Engineering at Southern Methodist University, Dallas, Texas. Her main research interests include III-V optoelectronics design and development, photonic switching, WDMOTDM technologies and high-speed optical testing. Dr. Shi has over 20 publications in various technical journals and conferences.

PLACE PHOTO HERE

Gary Evans Gary A. Evans (S'74-M'75-SM'82-F'92) was born in Omak, WA. He received the B.S.E.E. degree from the University of Washington, Seattle, in 1970 and the M.S.E.E. and Ph.D. degrees in electrical engineering and physics from the California Institute of Technology (Caltech), Pasadena, in 1971 and 1975. After a postdoctoral year at Caltech, he worked for R&D Associates, Marina Del Rey, CA, and was a Visiting Assistant Professor in the Electrical Engineering Department at the University of Washington (1977-1979). He has worked at the Aerospace Corporation, El Segundo, CA (1979-1981), TRW, Redondo Beach, CA (1981-1984), and RCA Laboratories (now Sarnoff Corporation), Princeton, NJ (1984-1992). In 1992, he joined Southern Methodist University, Dallas, TX, as a Professor in the Electrical Engineering Department. He is a founder and member of the board of directors of Photodigm. Since 1979, he has primarily worked on the design, growth, and fabrication of conventional cleaved facet and grating surface emitting semiconductor lasers. He has over 240 publications, 20 patents, and is a co-editor of the book Surface Emitting Semiconductor Lasers (New York: Academic Press, 1993). He is a licensed professional engineer. Dr. Evans was elected a Fellow of the IEEE for "contributions to the development, fabrication, and understanding of semiconductor lasers." He has served on numerous IEEE committees, is a past Chairman of the Princeton, NJ, and Dallas, TX Sections of the Lasers and Electro-Optics Society (LEOS), a past Chairman of the Santa Monica Bay Section of the IEEE, was an Associate Editor of the IEEE Journal Of Quantum Electronics (1989-1995), was the Finance Chairman for the 1994 IEEE International Semiconductor Laser Conference, and was a Technical Program Vice Chair for the 1996 International Communications Conference.

PLACE PHOTO HERE

Jerome Butler Jerome Butler (F'90) was born in Shreveport, Louisiana. He received the B.S.E.E. degree from Louisiana Polytechnic Institute, Ruston, and the M.S.E.E and Ph.D. degrees from the University of Kansas, Lawrence.

He was a Research Assistant and held a CRES Fellowship at the Center for Research in Engineering Sciences, University of Kansas. He conducted research concerned with electromagnetic wave propagation and the optimization and synthesis techniques of antenna arrays. He joined the faculty of the School of Engineering and Applied Science, Southern Methodist University, Dallas, Texas where he is now a University Distinguished Professor of Electrical Engineering. His primary research areas are solid state injection lasers, radiation and detection studies of lasers, millimeter-wave systems, integrated optics and the application of integrated optical circuits and quantum electronics. In 1977 he was given the Southern Methodist University Sigma Xi Research Award. In the summers from 1969 to 1990, he was a Staff Scientist, at the David Sarnoff Research Center (formerly RCA Laboratories), Princeton, NY. During the 1996-97 academic year he was on sabbatical leave with the Photonics and Micromachining System Components laboratory at Texas Instruments. He has held consulting appointments with Photodigm, the Photonics and Micromachining System Components laboratory at Texas Instruments, the Central Research Laboratory of Texas Instruments, Inc.,the Geotechnical Corporation of Teledyne, Inc., Earl Cullum Associates of Dallas, Texas and the University of California Los Alamos Scientific Loboratory, Los Alamos, New Mexico.

Dr. Butler is a member of Sigma Xi, Tau Beta Pi, Eta Kappa Nu, and is a registered professional engineer in the State of Texas. He was elected a fellow of the IEEE for his contributions to semiconductor lasers and the radiation characteristics of optical waveguides.